Indirect Dissociative Recombination of LiH$^+$ Molecules Fueled by Complex Resonance Manifolds

R. Čurík* and Chris H. Greene

Department of Physics and JILA, University of Colorado, Boulder, Colorado 80309-0440, USA
(Received 17 January 2007; published 26 April 2007)

The LiH$^+$ molecule is prototypical of the *indirect* dissociative recombination (DR) process, in which a colliding electron destroys the molecule through Rydberg capture pathways. This Letter develops the first quantitative test of the Siegert state multichannel quantum-defect theory description of indirect DR for a diatomic molecular ion. The *R*-matrix approach is adopted to calculate *ab initio* quantum defects, functions of the internuclear distance that characterize both Rydberg states and the zero-energy collisions of electrons with LiH$^+$ ions. We identify the doorways to fast indirect DR as complex resonance manifolds, which couple closed channels having both high and low principal quantum numbers. This sheds new light on the competition between direct and indirect DR pathways and suggests the reason previous theory underestimated the DR rate by an order of magnitude.

The LiH molecule was one of the first participants in early Universe chemistry, and it played a key role in the cooling of primordial gases. Therefore, the relative abundance of LiH and its formation process have drawn significant attention in models of the Universe. Stancil *et al.* [1] noticed that direct radiative association of neutral atoms, Li + H → LiH + ν, occurs at the very slow rate coefficient of $\sim 10^{-20}$ cm^3 s^{-1}.

On the other hand, radiative association with ionic hydrogen Li + H$^+$ → LiH$^+$ + ν is predicted to occur [2,3] at the much higher rate of $\sim 10^{-15}$ cm^3 s^{-1}. The resulting LiH$^+$ and LiH abundances are controlled by photoionization, collisions, and dissociative recombination (DR) with free electrons. A recent DR experiment for LiH$^+$ [4] has measured the DR rate coefficient for collisions at $T = 139$ K (12 meV) to be $(6 \pm 2) \times 10^{-7}$ cm^3 s^{-1}. From numerous *ab initio* calculations of the LiH and LiH$^+$ potential surfaces [5–10], there is no Born-Oppenheimer neutral state that crosses the ionic ground state potential curve anywhere near the ionic minimum. Thus, the high measured DR rate for such an *indirect* or *noncrossing* process is challenging to reconcile with existing theoretical results. The rate coefficient estimated theoretically in Ref. [1] is 2.6×10^{-8} cm^3 s^{-1}. Another theoretical study by Florescu *et al.* [10] applied multichannel quantum-defect methods with the relevant nonadiabatic coupling elements obtained from a generalized Hellmann-Feynman theorem [11] to calculate that the 139 K DR rate coefficient should equal 3.6×10 cm^3 s^{-1}. Since both of these theoretical studies underestimate the DR rate for this simple diatomic by more than an order of magnitude, it shows that the proper physical description of the underlying mechanism for indirect DR processes continues to challenge our theoretical understanding.

Quantum-defect theory in connection with frame transformation into a basis of Siegert vibrational states [12,13] has shown promise in describing DR for a model diatomic [14] and for the triatomic H$_3^+$ molecule [15], systems for which indirect Rydberg state pathways dominate. But to date there has been no rigorous test of the Siegert-state-based multichannel quantum-defect theory (MQDT) formulation for an experimentally studied system for which the relevant quantum-defect matrices have been determined directly in an *ab initio* scattering-type calculation. Accordingly, the main goal of the current Letter is to analyze dissociative collisions between a low-energy electron and the LiH$^+$ ion, as a fundamental prototype system that provides a stringent test of this combination of theoretical elements: *R*-matrix theory, MQDT, and frame-transformation theory based on Siegert pseudostates [16–19].

The body-fixed adiabatic eigenquantum defects $\mu_\gamma^\Lambda(R)$ are related to the energy differences (in a.u.) between the potential curves of the ion $U^+(R)$ and the neutral Rydberg states $U_{n\gamma}^\Lambda(R)$ by Mulliken's equation

$$U_{n\gamma}^\Lambda(R) = U^+(R) - \frac{1}{2[\nu_\gamma^\Lambda(R)]^2}, \qquad (1)$$

where the effective quantum number $\nu_\gamma^\Lambda(R) = n - \mu_\gamma^\Lambda(R)$, and Λ denotes the projection of the Rydberg electron angular momentum l onto the axis of the diatomic molecule. Of course, l is not a good quantum number, so γ is an eigenindex distinguishing different Rydberg series of LiH. Fundamentally, body-frame quantum defects are represented by a matrix $\mu_{ll'}^\Lambda(R)$ with different partial waves coupled by off-diagonal elements, after which the $\mu_\gamma^\Lambda(R)$ are obtained as its eigenvalues. *Ab initio* potential energy surfaces by themselves provide no direct information about off-diagonal couplings or, equivalently, about the eigenvectors $U_{l\gamma}(R)$, and many authors tend to neglect them [10] or estimate them using a two-channel Landau-Zener curve-crossing formula [20] or sometimes by fitting them in a diabatic representation [21].

But the present study exploits the familiar MQDT theorem [18] that smoothly connects quantum defects (multiplied by π) at energies just below the ionization threshold to R-dependent short-range scattering phase shifts (or multichannel scattering or reaction matrices) just above the threshold:

$$\pi \mu_{ll'}^{\Lambda}(R) = \sum_{\gamma} U_{l\gamma}(R) \delta_{\gamma}^{\Lambda}(R) U_{l'\gamma}(R). \quad (2)$$

Here $\delta_{\gamma}^{\Lambda}$ are the low- or zero-energy eigenphases for $e^- +$ LiH$^+$ collision, and the eigenvector matrix is $\underline{U}(R)$, which transforms the short-range K-matrix into diagonal form. We used the diatomic R-matrix package [22] to calculate the short-range K matrix by matching to Coulomb functions at an R-matrix boundary of $r_0 = 25a_0$. The target was described by an augmented valence triple-zeta Slater-type orbital basis set [23]. From the calculated $^1\Sigma^+$ and $^3\Sigma^+$ quantum defects shown in Fig. 1, the s-wave quantum defect is only weakly perturbed from its Li$^+$ limit of 0.399, over a wide range of internuclear distances. Thus, coupling to nuclear motion will be controlled by higher partial waves, namely, p and d waves. The $^1\Pi$ and $^3\Pi$ quantum defects have been calculated to be an order of magnitude smaller, and they have negligible impact on the final DR results.

The internuclear distance R is a good body-frame "quantum number" when all electrons are confined within the box specified by r_0 and the Born-Oppenheimer approximation is strictly valid. The vibrational frame transformation connects R with the laboratory-frame quantization of this degree of freedom expressed by vibrational wave functions $\phi_{jv}(R)$. Siegert pseudostates [12,13] provide a unified description of the bound vibrational states and the vibrational continuum. In the present case, they solve the vibrational Schrödinger equation and boundary

conditions:

$$\left[-\frac{d^2}{dR^2} + 2MU^+(R) + \frac{j(j+1)}{R^2} - k_{jv}^2 \right] \phi_{jv}(R) = 0, \quad (3)$$

$$\phi_{jv}(0) = 0; \left(\frac{d}{dR} - ik_{jv} \right) \phi_{jv}(R)|_{R_0} = 0. \quad (4)$$

In the above equations, j is a rotational quantum number of the ion, and M stands for its reduced mass, while R_0 denotes a nuclear radius beyond which we approximate the interaction potential in (3) to be constant and $\phi_{jv}(R) = \exp(ik_{jv}R)$ for $R \geq R_0$. Figure 2 shows an example of the $j = 0$ Siegert state momentum eigenvalue distribution. Because the nuclei are confined within $R_0 = 10a_0$, we obtain only 4 bound states, in contrast with the expected total of 7 bound states found in Refs. [6,10]. However, for the lower vibrational levels that fit inside, agreement in the level spacing is achieved within 2 cm^{-2}.

Because the orthogonality relation between two different Siegert pseudostates is slightly modified [13], a surface term [14] is added to the standard frame-transformation integral [24], yielding

$$S_{lv,l'v'}^{\Lambda}(j, j') = \int_0^{R_0} dR \phi_{jv}(R)(e^{2i\pi\underline{\mu}^{\Lambda}(R)})_{l,l'} \phi_{j'v'}(R)$$
$$+ i \frac{\phi_{jv}(R_0)(e^{2i\pi\underline{\mu}^{\Lambda}(R_0)})_{l,l'} \phi_{j'v'}(R_0)}{k_{jv} + k_{j'v'}}. \quad (5)$$

The underline in this equation denotes that $\underline{\mu}^{\Lambda}$ is a matrix with indices $\mu_{ll'}^{\Lambda}(R)$. Moreover, the rotational indices (j, j') of this body-frame $\underline{S}$ matrix do not give rotational transition probabilities—they serve only as a reminder that the vibrational functions exhibit a j dependence through the centrifugal term in Eq. (3). To reiterate, the rotational frame transformation transforms a set of body-frame quantum numbers (l, Λ, J) into a set of laboratory-frame quantum numbers (l, j, J). The total angular momentum J is defined via $\boldsymbol{J} = \boldsymbol{l} + \boldsymbol{j}$. The LiH$^+$ ion is treated in Hund's case (b), with spin-orbit coupling neglected.
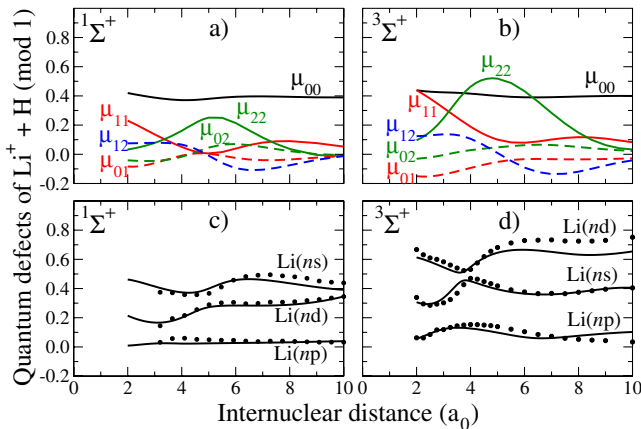

FIG. 1 (color online).   Upper panels: The calculated quantum-defect matrix elements are shown versus the internuclear distance—(a) singlets, (b) triplets. Lower panels: The solid curves are the eigenvalues of the matrices in (a) and (b). The black dots are eigenquantum defects extracted from $n = 4$ states in extensive bound state configuration-interaction calculations [10].
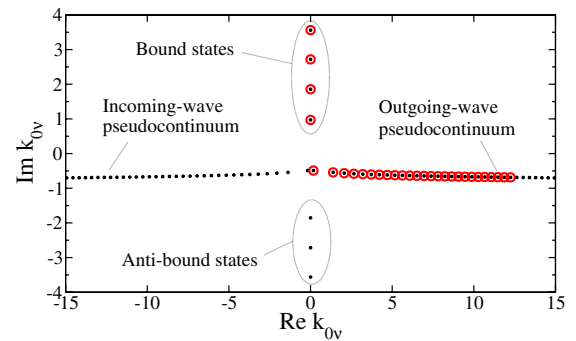

FIG. 2 (color online).   Distribution of the $j = 0$ Siegert momentum eigenvalues from Eqs. (3) and (4) in the complex plane. The circled states are the ones used in the calculations of this Letter.

Definite total parity $\eta = (-1)^{l+j}$ is also enforced, whereby the short-range laboratory-frame scattering matrix is

$$S^{J\eta}_{lj\nu,l'j'\nu'} = \sum_{\Lambda} U^{\Lambda\eta}_{Jjl} S^{\Lambda}_{\nu l,\nu' l'}(j,j') U^{\Lambda\eta}_{Jj'l'}. \qquad (6)$$

The real, orthogonal rotational transformation matrix $U^{\Lambda\eta}_{Jjl}$ is taken from Ref. [16] and will not be repeated here.

As is familiar in MQDT applications, the "short-range" or "unphysical" scattering matrix $\underline{S}$ in Eq. (6) is diagonal in the J and η quantum numbers. It represents an amplitude for electron-ion scattering from an initial channel defined by $(l'j'\nu')$ into a final channel defined by $(lj\nu)$, but some of these channels in $\underline{S}$ are typically closed energetically. The physically relevant S matrix is, of course, defined only in the open-channel space and is obtained by the "elimination of closed-channels" formula [17]:

$$\underline{S}^{\text{phys}} = \underline{S}^{oo} - \underline{S}^{oc}[\underline{S}^{cc} - e^{-2i\underline{\beta}(E)}]^{-1}\underline{S}^{co}, \qquad (7)$$

where the superscripts o and c, respectively, denote open and closed sub-blocks of the unphysical S matrix (6), and $\underline{\beta}(E)$ is a diagonal matrix of effective Rydberg quantum numbers with respect to the closed-channels thresholds:

$$\beta_{ij} = \frac{\pi\delta_{ij}}{\sqrt{2(E_i - E)}}. \qquad (8)$$

The total energy of the electron + ion system is E, and E_i is the ionization threshold for channel $i \equiv (\nu j l)$. Here, as in Refs. [14,15], the high ionization thresholds are described by a Siegert pseudocontinuum state with finite widths, so E_i and $\underline{\beta}(E)$ are *complex*. This fact alone destroys the unitarity of $\underline{S}^{\text{phys}}$, making it subunitary. The lost flux is associated with a trapped Rydberg electron in a closed channel that represents a high-lying vibrational state that is dissociative, with outgoing-wave character, and has a complex vibrational energy and a corresponding finite lifetime. The departure from unitarity was identified in Refs. [14,15] as the dissociation probability following electron impact in incident channel i':

$$\sigma^{J\eta}_{i'}(\varepsilon_{i'}) = \frac{\pi}{2\varepsilon_{i'}}\left[1 - \sum_i S^{\text{phys}}_{ii'}(E)S^{\dagger\text{phys}}_{i'i}(E)\right], \qquad (9)$$

with the incident electron collision energy $\varepsilon_{i'} = E - E_{j'\nu'}$. This cross section depends on the initial channel $i' = (\nu'j'l')$; the collision preserves the conserved quantum numbers $(J\eta)$. The experimentally observable cross section for dissociation following electron impact is then

$$\sigma_{j'\nu'}(\varepsilon_{j'\nu'}) = \frac{1}{2j'+1}\sum_{\eta J l'}(2J+1)\sigma^{J\eta}_{l'j'\nu'}(\varepsilon_{j'\nu'}). \qquad (10)$$

We further average over a Boltzmann distribution of initial rovibrational states of the ion at the temperature ($T = 300$ K) appropriate to the experiment [4]. The corresponding recombination rate $\alpha(E_c)$ is

$$\alpha(E_c) = \sqrt{2E_c}\,\sigma(E_c). \qquad (11)$$

This calculated DR rate exhibits an infinite number of resonances near each closed-channel ionization threshold, associated with autoionizing and predissociating states of LiH. To compare with the storage ring experiments [4], we must convolve over an anisotropic finite spread in the electron energy; the spread is different for the parallel ($\Delta E_\parallel = 0.1$ meV) and the much broader $\Delta E_\perp = 12$ meV perpendicular components of the relative velocity vector. The convolution over parallel and perpendicular energy distributions has been performed as was outlined in Ref. [15] and elaborated in detail in Ref. [25]. Figure 3 summarizes our results along with previous experimental and theoretical results. This figure also demonstrates the results of a numerical test conducted to interpret the discrepancy between our theoretical results and those of Ref. [10]. Specifically, we have performed one set of calculations that neglect the off-diagonal l mixing to mimic the calculations performed in Ref. [10], i.e., using only the diagonal eigenvalue form $\mu^{\Lambda}_\gamma(R)$ of quantum-defect matrix [shown in Figs. 1(c) and 1(d)]. Introduction of this approximation lowers the DR rate by an order of magnitude, and this artificially restricted calculation agrees with the results of Ref. [10]. Thus, the presence of R-dependent l mixing is crucial for this system. Moreover, the rate is predominantly controlled by d-wave collisions, whereas in Ref. [10] it was assumed that it was dominated by p waves.

We now identify the qualitative mechanism responsible for this high indirect DR rate. Figure 4 summarizes the probabilities of various DR pathways at an energy near the first vibrational threshold. For clarity, we have neglected rotations in this qualitative analysis, because we found very little effect of the rotational frame transformation on the present results at this energy resolution. In Fig. 4, no thermal averaging has been applied, and the LiH$^+$ ion is
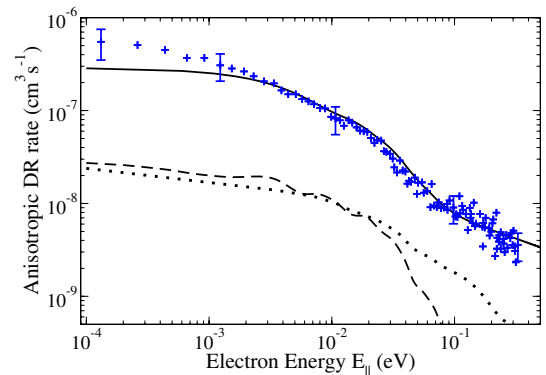
FIG. 3 (color online). DR rate: The solid curve is our calculated, anisotropically averaged rate for $\Delta E_\parallel = 0.1$ meV and $\Delta E_\perp = 12$ meV. The dashed curve shows the calculation from Ref. [10]. The dotted curve is our truncated result obtained by neglecting the off-diagonal couplings in the quantum-defect matrix (see Fig. 1). The crosses denote the experimental data [27], with a few characteristic error bars shown.
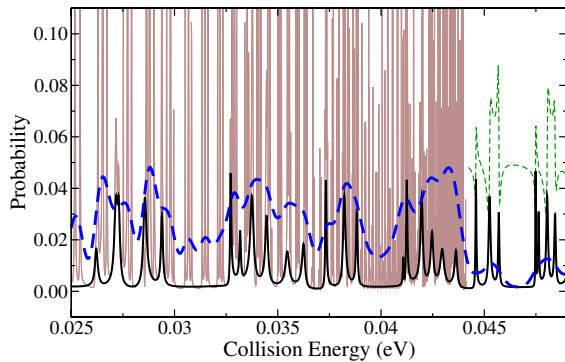
FIG. 4 (color online).   Contributions to DR probabilities are
shown as functions of energy near the first vibrational threshold:
The thick dashed curve represents the average DR probability.
The full spectrum of Rydberg resonances converging to the first
threshold is denoted by the thin line. Contributions from the
second and higher thresholds are shown as the thick solid curve.
The thin dashed curve is the probability of a vibrational excita-
tion process $v_0 \rightarrow v_1$, which is only energetically allowed above
the $v = 1$ threshold.

initially in the vibrational ground state. The DR probabil-
ities shown are the quantity inside the square brackets in
Eq. (9). The thick dashed curve denotes the average DR
probability across the threshold. The DR probability drops
from about 5% of the incident flux below the threshold
down to only 0.6% above the threshold. The DR probabil-
ity below the threshold is built up as the cumulative effect
of the dense forest of Rydberg resonances attached to the
first vibrationally excited state, seen as the thin solid curve.
The thick solid curve shows the contributions to DR proba-
bility when the incident electron is captured into Rydberg
states associated with higher vibrational thresholds.
Figure 4 also explains the reason the DR flux drops sharply
above the $v = 1$ threshold. The thin dashed curve shows
our calculated probability of vibrational excitation $0 \rightarrow 1$.
As can be noticed from the amplitudes for the probabilities
of both processes below and above the threshold, most of
the DR flux just below the threshold turns discontinuously
into vibrational excitation flux once that channel becomes
open. These results indicate that the DR process is con-
trolled by a doorway, namely, capture of the incident
electron into a Rydberg state attached to the first vibra-
tional threshold. However, if there is no higher-v or
lower-n perturbing level overlapping the total energy of
the collision complex, the electron will tend to autoionize
before DR can take place. Throughout the energy range of
a multichannel complex resonance, though, the initial cap-
ture can efficiently pump more energy into vibration at the
first electron recollision, and Fig. 4 shows that this resonant
perturbed Rydberg complex increases the DR rate by about
another factor of 3. This complex resonance mechanism for
indirect DR is believed to apply to many other systems that
are not controlled by the usual simple capture mechanism
into a dissociative state. A hint of its importance in H_3^+ DR

is evident across the energy range 110–160 cm^{-1} in Fig. 10
of Ref. [26].

*Corresponding author.
Electronic address: curik@colorado.edu

[1] P. C. Stancil, S. Lepp, and A. Dalgarno, Astrophys. J. **458,**
401 (1996).

[2] A. Dalgarno, K. Kirby, and P. C. Stancil, Astrophys. J.
458, 397 (1996).

[3] F. A. Gianturco and P. G. Giorgi, Astrophys. J. **479,** 560
(1997).

[4] S. Krohn *et al.*, Phys. Rev. Lett. **86,** 4005 (2001).

[5] A. Boutalib and F. X. Gadéa, J. Chem. Phys. **97,** 1144
(1992).

[6] H. Berriche and F. X. Gadéa, Chem. Phys. **191,** 119 (1995).

[7] F. Gemperle and F. X. Gadéa, J. Chem. Phys. **110,** 11 197
(1999).

[8] A. Yiannopoulou, G. H. Jeung, S. J. Park, H. S. Lee, and
Y. S. Lee, Phys. Rev. A **59,** 1178 (1999).

[9] S. N. Altunata and R. W. Field, Phys. Rev. A **67,** 022507
(2003).

[10] A. I. Florescu, A. Suzor-Weiner, T. Leininger, and F. X.
Gadéa, Phys. Scr. **T110,** 172 (2004).

[11] A. V. Stolyarov and M. S. Child, Phys. Rev. A **63,** 052510
(2001).

[12] A. J. F. Siegert, Phys. Rev. **56,** 750 (1939).

[13] O. I. Tolstikhin, V. N. Ostrovsky, and H. Nakamura, Phys.
Rev. A **58,** 2077 (1998).

[14] E. L. Hamilton and C. H. Greene, Phys. Rev. Lett. **89,**
263003 (2002).

[15] V. Kokoouline and C. H. Greene, Phys. Rev. A **68,** 012703
(2003).

[16] E. S. Chang and U. Fano, Phys. Rev. A **6,** 173 (1972).

[17] M. Aymar, C. H. Greene, and E. Luc-Koenig, Rev. Mod.
Phys. **68,** 1015 (1996).

[18] M. J. Seaton, Rep. Prog. Phys. **46,** 167 (1983).

[19] C. H. Greene and Ch. Jungen, Adv. At. Mol. Phys. **21,** 51
(1985).

[20] Å. Larson *et al.*, Phys. Rev. A **62,** 042707 (2000).

[21] Å. Larson, S. Tonzani, R. Santra, and C. H. Greene,
J. Phys.: Conf. Ser. **4,** 148 (2005).

[22] L. A. Morgan, C. J. Gillan, J. Tennyson, and X. Chen,
J. Phys. B **30,** 4087 (1997).

[23] I. Ema, J. M. Garcia de la Vega, G. Ramirez, R. Lopez,
J. Fernandez Rico, H. Meissner, and J. Paldus, J. Comput.
Chem. **24,** 859 (2003).

[24] C. H. Greene and Ch. Jungen, Phys. Rev. Lett. **55,** 1066
(1985).

[25] V. Kokoouline and C. H. Greene, J. Phys.: Conf. Ser. **4,** 74
(2005).

[26] V. Kokoouline and C. H. Greene, Phys. Rev. A **69,** 032711
(2004).

[27] S. Krohn, Ph.D. thesis, the Combined Faculties for the
Natural Sciences and Mathematics of the Ruperto-Carola
University of Heidelberg, Germany, 2001, p. 102.